High Redshift Type Ia Supernova Rates

N. Kuznetsova[1], K. Barbary[1,2], A. G. Kim[1], R. Pain[3], N. A. Roe[1], G. Aldering[1], R. Amanullah[1], K. Dawson[1], M. Doi[4], V. Fadeyev[5], A. S. Fruchter[6], R. Gibbons[7], G. Goldhaber[1,2], A. Goobar[8], N. Kashikawa[9], R. A. Knop[7], M. Kowalski[10], C. Lidman[11], J. Meyers[1,2], T. Morokuma[4], S. Perlmutter[1,2], D. Rubin[1,2], D. J. Schlegel[1], A. L. Spadafora[1], V. Stanishev[8], M. Strovink[1,2], N. Suzuki[1], L. Wang[12], N. Yasuda[13]

February 27, 2007

ABSTRACT

We present a new measurement of the Type Ia supernova (SN) rates up to a redshift of 1.7 using the Hubble Space Telescope (HST) GOODS data combined with an HST dataset covering the North GOODS field collected in 2004. The latter data consist of four observational epochs separated by a typical time period of ∼45 observer-frame days, and the data were taken in two broadband ACS filters: F775W and F850LP. We use a Bayesian approach for identifying type Ia supernova and derive a volumetric SN Ia rate as a function of redshift, assuming a ΛCDM cosmology and an $H_0 = 70 \times h_{70}$ (km/s) Mpc^{-1}. We fit this rate to a two-component model, in which one fraction of type Ia supernovae traces the instantaneous star formation history (SFH); and the other, the current mass density. Our results indicate that the latter contribution is consistent with zero, and that the best-fitting model points to an increase of the type Ia supernova rates with redshift proportionally to the instantaneous SFH.

[1]E. O. Lawrence Berkeley National Laboratory, 1 Cyclotron Rd., Berkeley, CA 94720, USA

[2]Department of Physics, University of California Berkeley, Berkeley, 94720-7300 CA, USA

[3]LPNHE, CNRS-IN2P3, University of Paris VI & VII, Paris, France

[4]Institute of Astronomy, School of Science, University of Tokyo, Mitaka, Tokyo, 181-0015, Japan

[5]UCSC (NEED ADDRESS)

[6]Space Telescope Science Institute, 3700 San Martin Drive, Baltimore, MD 21218, USA

[7]Department of Physics and Astronomy, Vanderbilt University, Nashville, TN 37240, USA

[8]Department of Physics, Stockholm University, Albanova University Center, S-106 91 Stockholm, Sweden

[9]National Astronomical Observatory, Mitaka, Tokyo 181-0058, Japan

[10]Humboldt University (NEED ADDRESS)

[11]European Southern Observatory, Alonso de Cordova 3107, Vitacura, Casilla 19001, Santiago 19, Chile

[12]Texas A&M (NEED ADDRESS)

[13]Institute for Cosmic Ray Research, University of Tokyo, Kashiwa, 277 8582 Japan

1. Introduction

The discovery of the dark energy component of the Universe (Perlmutter et al 1997; Riess et al. 1998) is one of the most profound and consequential experimental breakthroughs of modern physics. The empirical evidence for the existence of dark energy came from observations of type Ia supernovae, which are believed to be thermonuclear explosions of a progenitor white dwarf after it has reached the Chandraseckhar mass limit (Chandrasekhar 1931). However, the physics of type Ia supernova production is not well understood. The two most plausible scenarios for the white dwarf to accrete the necessary mass are the single degenerate case, where the white dwarf is located in a binary system with a red giant companion star; and the double degenerate case, where two white dwarfs merge. The type Ia supernova rate is correlated with the star formation history (SFH), and thus a measurement of the rate as a function of redshift helps constrain the possible type Ia progenitor models.

In addition to its importance for understanding type Ia supernovae as astronomical objects, a good grasp of the type Ia supernova rate to high redshifts is important for the next generation of space-based supernova cosmology experiments, such as SNAP (Aldering et al. 2003). Studies show (Linder and Huterer 2003) that if realistic systematic errors are properly taken into account, the optimal supernova sample will have a redshift range with maximum $z_{\rm max} > 1.5$. It is therefore of great practical interest to determine the rates of type Ia supernovae at redshifts > 1.

The subject of type Ia supernova rates has been addressed by many authors in the past. Existing rate measurements have been mostly limited to redshift ranges < 1: the results of Cappellaro et al. (1999), Hardin et al. (2000), Madgwick et al. (2003), and Blanc et al. (2004) measure the rates at redshifts $\leq \sim 0.1$; Neill et al. (2006) and Pain et al. (2002), at intermediate redshifts of 0.47 and 0.55, respectively; and Barris and Tonry (2006), up to a redshift of 0.75. The only published measurement of the rates at redshifts > 1 is that of Dahlen et al. (2004), who analyzed the GOODS dataset. There are several main differences that distinguish our work from that of Dahlen et al. (2004). First, we augment the GOODS sample with the HST data collected during the Spring - Summer 2004 high redshift supernova searches. Second, we adopt a novel approach to typing supernovae, using photometric data alone and a Bayesian probability method described in Kuznetsova and Connolly (2006). This method can be particularly useful for the large upcoming ground-based surveys where it may not be feasible to obtain a spectral confirmation of the supernova type for each candidate. Third, our method of calculating the control time (the time during which a supernova search is potentially capable of finding supernova candidates) and the efficiency of identifying supernovae is quite different.

The paper is organized as follows. In Section 2, we describe the data samples used in the analysis. In Section 3 we describe the supernova candidate identification and typing process. The number of supernova candidates used for the analysis is derived in Section 4.2, Section 4.1 explains the control time and survey area calculation, and the predicted vs. observed numbers of supernovae for different models of the type Ia supernova rate are computed in Section 4.3. We also

describe the implications for constraining the type Ia supernova progenitor models in this section. A comparison of the rates with those reported in literature is given in Section 4.4. Conclusions are given in Section 5.

2. Data Sample

For this analysis, we use the Hubble Space Telescope (HST) GOODS dataset collected in 2002-2003 (Renzini et al. 2002; Dickinson et al. 2003; Giavalisco et al. 2004). In addition to the GOODS data, we use an HST sample collected in the Spring-Summer of 2004, which hereafter we will call the Search2004 sample. The GOODS dataset consists of five epochs (data taking periods), separated by approximately 45 observer-frame days. The GOODS data used for this analysis were taken in two HST ACS filter bands: F775W (centered at 775 nm) and F850LP (centered at 850 nm)[14]. Each F850LP image consists of four exposures; and each F775W image, of two. The GOODS survey includes two fields, GOODS North and GOODS South, and cover approximately 320 square arcminutes. The fields are sub-divided into smaller "tiles" (typically 15 or 16), as shown in Fig. 1.

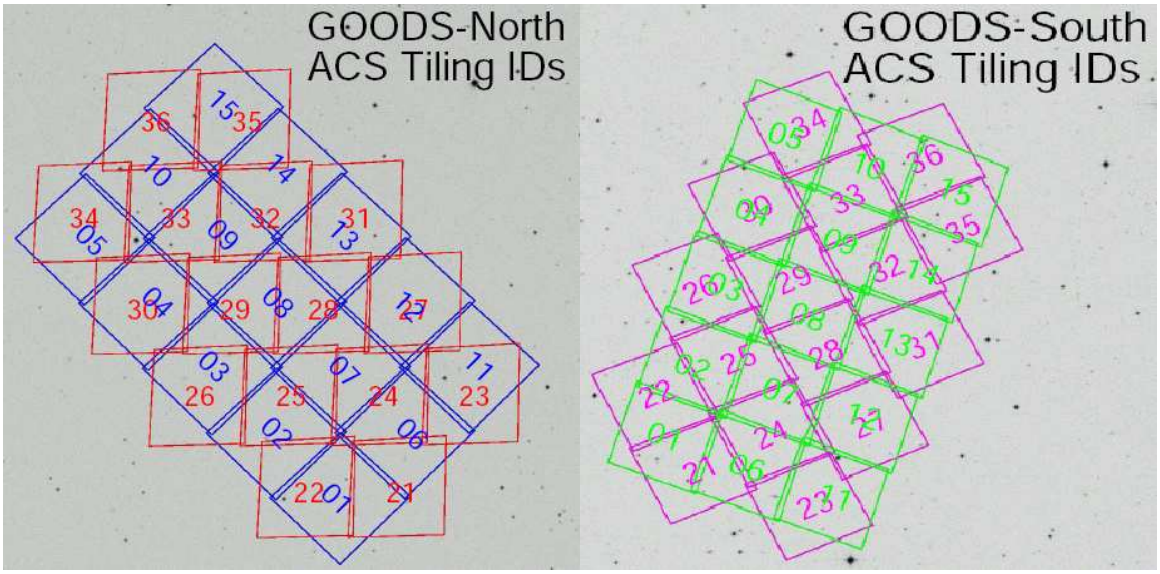

Fig. 1.— The North (left) and South (right) GOODS fields. The fields are subdivided into tiles, which are shown (along with their ID numbers) on the figures. The size of a single tile is ∼11.5 sq. arcmin.

The Search2004 HST supernova dataset covers only the GOODS North field, with the same

[14]The ACS filter transmission curves are available at http://acs.pha.jhu.edu/instrument/filters/.

tiling as that of the GOODS North dataset. It consists of 4 epochs separated by approximately 45 observer-frame days. The data in this sample were taken in two HST ACS passbands: F775W and F850LP, with one exposure for every F775W image and four for every F850LP image. For convenience, a summary of the datasets used is given in Table 1.

Epoch	Filter	Exp.time (s)	Filter	Exp. time (s)	# Tiles	Taken On
GOODS South						
1	F775W	1040	F850LP	2120	15	7/31 - 8/4 (2002)
2	F775W	1040	F850LP	2120	16	9/19 - 9/22 (2002)
3	F775W	1040	F850LP	2120	15	10/31 - 11/3 (2002)
4	F775W	1040	F850LP	2120	16	12/19 - 22 (2002)
5	F775W	1040	F850LP	2120	15	2/1 - 2/5 (2002)
GOODS North						
1	F775W	1120	F850LP	2400	14	11/21 - 11/22 (2002)
2	F775W	1000[a]	F850LP	2120	17	1/2 - 1/4 (2003)
3	F775W	960	F850LP	2060	16	2/20 - 2/23 (2003)
4	F775W	960	F850LP	2000	14	4/3 - 4/6 (2003)
5	F775W	960	F850LP	2080	15	5/21 - 5/25 (2003)
Search2004 Sample (GOODS North tiles)						
1	F775W	400	F850LP	1600	15	4/2 - 4/4 (2004)
2	F775W	400	F850LP	1600	15	5/20 - 5/23 (2004)
3	F775W	400	F850LP	1600	15	7/9 - 7/10 (2004)
4	F775W	400	F850LP	1600	15	8/26 - 8/28 (2004)

[a]except for tile 30 (1060)

Table 1: A summary of the datasets used in this analysis, listing the data taking epochs, the filters, the exposure times of the combined exposures (in seconds), the number of GOODS field tiles, and the dates when the data were taken.

It is worth emphasizing that we are using photometric information from only two filter bands, providing one color measurement. The GOODS dataset has been analyzed before, and a number of supernovae (28 out of 42) were found and spectroscopically typed (Riess et al 2004; Strolger et al. 2004). For the Search2004 sample, however, the spectroscopic information is available only for a small fraction of the candidates. We treat both GOODS and Search2004 datasets in a consistent fashion, using photometric information only.

We start with the data that have been flat-fielded and gain-corrected by the HST pipeline, and use MultiDrizzle (Fruchter and Hook 2002) to perform cosmic ray rejection and to combine dithered observations. Drizzling is ineffective for the F775W data from the Search2004 sample, since they

contain only a single exposure for each GOODS North tile. We therefore use a morphological cosmic ray rejection package (Van Dokkum 2001) to create images with identifiable objects, thus allowing us to generate the geometrical transformations between images; however, the original images are used for extracting photometric information.

Supernovae are identified by subtracting a reference image from each of the HST search epochs. We create four distinct samples summarized in Table 2, which we use for identifying and performing simple aperture photometry on the supernova candidates in each of the five (four) epochs in the GOODS (Search2004) dataset. To obtain the multi-epoch photometry for the GOODS North data (sample #1), we combine all four epochs of the Search2004 sample and then subtract these data from each of the five North GOODS epochs in turn. For sample #2, we combine the entire North GOODS sample and subtract these data from each of the four Search2004 epochs in turn. Because the GOODS and Search2004 data were taken with a time separation of approximately a year, these samples should be sensitive to the supernovae that were both on the rise and on the decline during the GOODS (Search2004) data taking period for sample #1 (#2). For the GOODS South sample, however, we do not have any additional datasets, and are thus forced to separate the sample into two. This is the reason the three initial data samples (GOODS North and South and the Search2004 data set) result in four search samples. We combine South epochs 4 and 5 for sample #3, and epoch 1 and 2 for sample #4; we then subtract the two combined samples separately from each of the five South GOODS epochs. If a supernova candidate has been found in both samples #3 and #4, we

Sample #	Reference Dataset	Supernova Search
1	Combined Search2004 data (4 epochs)	Individual North GOODS epochs
2	Combined North GOODS data (5 epochs)	Individual Search2004 dataset epochs
3	Epochs 4+5 of the South GOODS data	Individual South GOODS epochs
4	Epochs 1+2 of the South GOODS data	Individual South GOODS epochs

Table 2: The samples used in our supernova search. To identify and extract photometry for supernova candidates, we subtract the data listed in column 2 from the data listed in column 3. Note that sample #2 has the deepest references.

consider it belonging to the sample in which it had an epoch with the largest signal-to-noise ratio. This avoids any possible double-counting of the candidates for the GOODS South data.

3. The Supernova Candidate Selection and Typing

The search for supernova candidates and their subsequent typing as Ia's is a 3-stage process:

1. First, supernova candidates are flagged by the software that is used to subtract the supernova search data from the reference data. The initial candidate selection is done using the

F850LP data only, because the search data are typically deeper in this filter than in F775W (see Table 1) and because F850LP covers supernova redshifts up to ∼1.5. The initial supernova selection (described in detail below) is quite generous and is primarily directed toward reducing the number of false positives resulting from various image processing artifacts and residual cosmic ray contamination. It is followed by a manual scan to reject any obvious remaining cosmic rays and image processing artifacts.

2. For the candidates that passed the first stage of the selection process, we use the multi-epoch F850LP and F775W data and require that the candidate's signal-to-noise ratio (SNR) in the subtracted data be greater than 2 for at least 3 search epochs, including at least two with a SNR greater than 3.

3. The final step is a Bayesian likelihood technique that assigns each candidate a probability to be a type Ia supernova.

For convenience, we summarize the selection process in Table 3. We now describe each of the selection stages in detail.

Selection Stage	Data Used	Cuts Applied
1	F850LP single (discovery) epoch	$SNR_{exposure} > 3$ in 4 exposures "mini-subtraction" consistency in 3 out of 4 exposures Percent increase $\geq 15\%$ in combined exposures shape cuts in combined exposures
2	F850LP, F775W, all epochs	≥ 3 epochs with S/N > 2 (incl. ≥ 2 epochs with S/N > 3)
3	F850LP, F775W, all epochs	Bayesian type Ia classification

Table 3: A summary of the type Ia supernova selection and typing process. The meaning of the cuts is explained in the text describing the corresponding stages.

3.1. Stage 1: Single Epoch Supernova Candidate Selection

In the first step of the supernova search, we search for supernova candidates in the individual epochs of the F850LP data by looking for signal in the reference-subtracted search images. The reference image is the same for each exposure (recall that each F850LP image consists of four exposures, each with the same exposure time), but different references may have different depths as described later. We use a simple aperture photometry with a radius of 3 pixels, where the pixel scale is 0.03", and apply the following cuts:

1. To eliminate variable objects that are not supernovae (such as cosmic rays), we do the following:

   - We start with considering the four individual exposures of the search images, before combining the exposures together or subtracting them from the reference image. The SNR measured for a supernova candidate in each of these exposures ($SNR_{exposure}$) should be at least 3. A false positive resulting from cosmic rays will likely not be present in every individual exposure.
   - We now subtract each of the individual exposures from the reference image at the location of the supernova candidate and compare the signal to the quadratic sum of the noise. The difference in these SNRs between the exposures must be < 3 for at least 3 out of 4 exposures. We are thus allowing one (and only one) of the four exposures of the search image to be contaminated by a cosmic ray.

2. Subtracting the combined exposures of the search data from the reference data, we require that:

   - The absolute value of the flux within the supernova candidate's aperture in the subtracted data divided by the flux in the reference data (the "percent increase" variable) be $\geq 15\%$.
   - The candidate's shape in the subtracted data must be consistent with a point source: we require that the candidate's full width in both x- and y- directions be < 4 pixels, and that the absolute value of its normalized xy moment be < 0.5 pixels.

Our search identified all of the supernovae found in the GOODS data by Riess et al (2004). As a sanity check, we verified that the measured magnitudes for these supernovae agree with those listed in Riess et al (2004). We find that in both F850LP and F775W, the magnitudes agree to $\sim$2-3% for magnitudes < 27. Additionally, we verified that the photometric extraction procedure is working well by creating "fake" supernovae and comparing their input and output magnitudes; they agree at a sub-percent level. It must also be noted that precision photometry is not crucial for the rates analysis, since the photometric measurements only matter for identifying the supernovae, and the errors resulting from the identification procedure itself, combined with the fact that we are considering a small sample, far outweigh the contribution from the photometric uncertainties.

All of these cuts are tuned and their efficiency is determined by a Monte Carlo procedure described below. They eliminate close to 90% of false detections. Obvious cosmic rays or image processing artifacts that manage to pass these cuts are rejected by a manual screening, with any questionable candidates left in the sample. The efficiency of the manual scan has been checked using a sample of $\sim$100 fake supernovae and 100% were correctly identified. The preliminary selection flags any variable objects – supernovae of various types, as well as active galactic nuclei (AGNs), *etc.* In Section 3.3, we describe our approach to selecting type Ia supernovae from the sample.

In order to understand the cuts used to select supernova candidates, as well as check the efficiency of the selection, we developed a Monte Carlo simulation that puts fake supernovae on real F850LP images. The technique follows the approach outlined in Pain et al. (2002) and works as follows.

First, we run SExtractor (Bertin and Arnouts 1996) v2.3 on the search images that have been combined, or drizzled, together from the individual exposures. We do this for a number of both North and South GOODS tiles. Using SExtractor's classification of objects as galaxies and stars, we create a list of the all of the galaxy positions on the image. Because in our analysis we are ignoring candidates near image edges, the galaxies located within 2 galaxy full widths at half maximum (also determined by SExtractor) from the image boundaries are discarded. The fake supernova that is to be put on the image is randomly assigned a magnitude that is drawn from a flat distribution between 23 to 30. The supernova's position is drawn from a Gaussian distribution with half the galaxy's full width at half maximum as the standard deviation and centered on the galaxy's nominal center. We then use STSDAS[15] *tranback* function to convert the fake supernova positions on the drizzled images into coordinates on the raw individual exposures. Fake supernovae themselves are created using the TinyTim software (Krist and Hook 2004), for the ACS WFC1 camera, in filter F850LP. The fake supernova signal, combined with a noise generated using a Poisson distribution with the signal's mean, is added onto the input exposures, which are subsequently processed in exactly the same way as real data are.

The fake supernovae that pass the preliminary selection of supernovae described above are compared with the input list of fakes. This allows us to calculate the efficiency of the selection cuts for the preliminary supernova selection. This efficiency is shown in Fig. 2 (upper left) as a function of the candidates' SNR on the reference-subtracted search images. Note that our reference images are not uniformly deep: they consist of 2, 4, or 5 combined epochs, depending on the tile of the GOODS field and the supernova's position on the tile (see Fig. 1). Figure 2 (upper right) shows the supernova finding efficiency as a function of the SNR for two representative cases: one, for all locations where two epochs contribute to the reference data; and other, for all locations where there are four epochs that are available for the reference data. We refer to these cases as "depth 2" and "depth 4", respectively. It is evident that, within errors, for a given SNR, the efficiency is virtually independent of the depth of the reference image at the location of the fake supernovae. We thus use the efficiency curve in Fig. 2 (upper left) that combines all of the depths, which we fit to the following four-parameter function:

$$\epsilon(SNR) = p_1 + \frac{p_2}{1 + e^{p_3\,(SNR - p_4)}} \tag{1}$$

where we obtain $p_1 = 0.96$, $p_2 = -18.04$, $p_3 = 0.41$, and $p_4 = -1.34$. The resulting fit is also shown in Fig. 2 (upper left).

[15]STSDAS and PyRAF are products of the Space Telescope Science Institute, which is operated by AURA for NASA

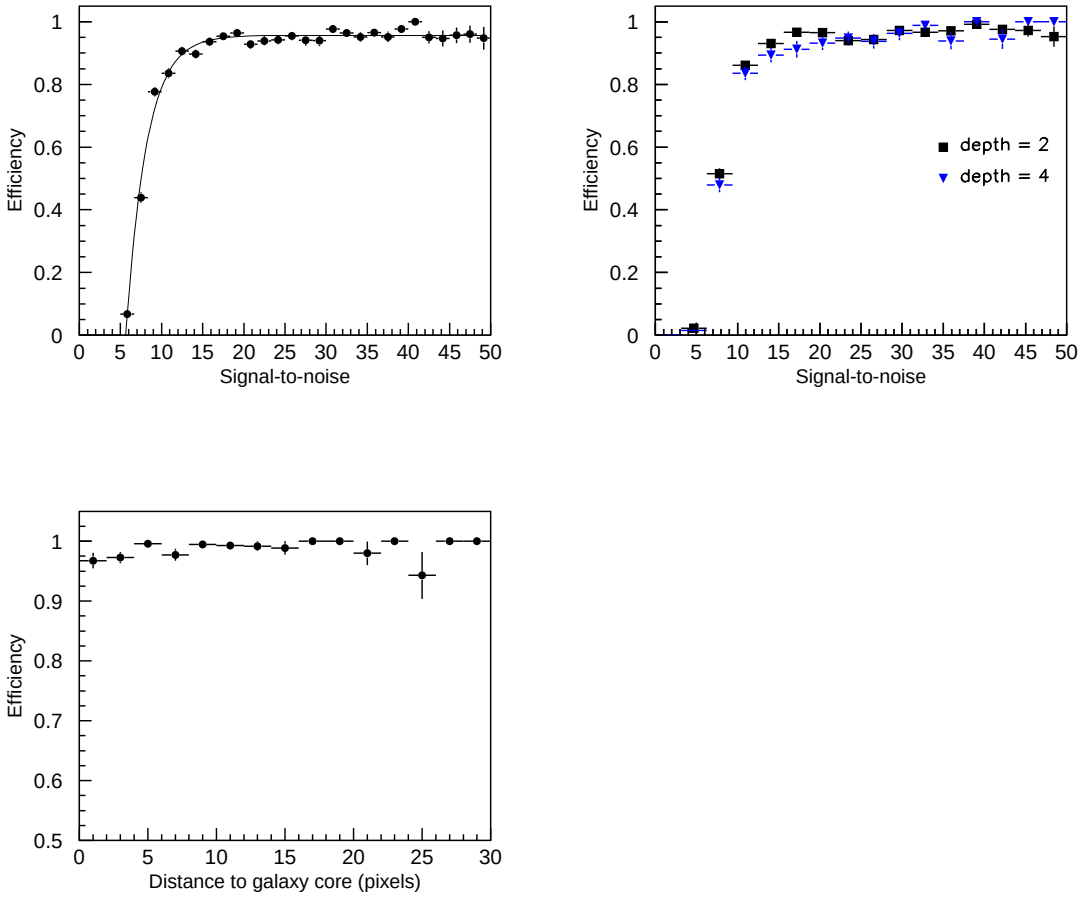

Fig. 2.— The efficiency of the stage 1 supernova selection in the reference-subtracted search images. The errors are assigned using the binomial statistics. The upper left plot shows the combined efficiency for all depths (see text for the definition of depth) of the reference image as a function of the candidate's SNR. Overlaid as a solid line is the fit of the efficiency to the function in Eqn. 1. The upper right plot shows the efficiencies for two representative depths: 2 (squares) and 4 (down turned triangles). The lower left plot shows the efficiency as a function of the supernova distance from the host galaxy core for all candidates with SNR > 15.

One concern in supernova searches is the potential loss of candidates located close to the core of their host galaxies. Figure 2 (lower left) shows the efficiency as a function of the supernova's distance from the core for all candidates with a SNR > 15. It is apparent that the efficiency remains essentially flat.

The efficiency parametrization given in Eqn. 1 is used in the control time calculation, as described in Section 4.1. The stage 1 selection efficiency is thus built into the control time.

3.2. Stage 2: The Multi-Epoch Selection

The second stage of the supernova candidate selection is where we turn to the multi-epoch photometric data in both filters. Subtracting the combined exposures of the search data from the reference data, we calculate the candidates' SNRs in the subtracted data and require that there be at least three epochs with a SNR > 2, including at least two epochs with the SNR > 3. These cuts are designed to eliminate candidates without at least somewhat reasonably well measured light curves. Because the Bayesian technique described in 3.3 provides a powerful discrimination of type Ia supernovae, these cuts can be very loose. At the end of stage 2, we have 27 candidates in sample #1, 17 candidates in sample #2, 12 candidates in sample #3, and 10 candidates in sample #4, for a total of 66 candidates. A list of these 66 candidates is given in Tables 4, 5, 6, and 7, for samples #1, #2, #3, and #4, respectively. All of these candidates have redshifts obtained from Strolger et al. (2004), the NASA/IPAC Extragalactic Database (NED) catalog[16], the Team Keck Treasury Redshift Survey (TKRS) catalog (Wirth 2004), or via private communications (Mobasher and Dahlen 2004). The typical redshift error for a spectroscopic redshift is taken to be 0.5%; and for a photometric redshift, 10%. If the redshift error of the candidate is not known, we assume a photometric error of 10%. The source of the redshift errors is listed in the tables as well. Precision photometric measurements for these candidates will be made available in Suzuki et al. (2007).

The stage 2 cuts are built into the calculation of the control time, as described in Section 4.1. The control time therefore naturally incorporates the efficiency of this selection.

3.3. Stage 3: The Identification of Type Ia Supernovae

The candidates that have been selected in stages 1 and 2 are assumed to be real transient objects, most likely supernovae, and must now be classified by type. With only scarce photometric data available, we turn to the Bayesian method of classifying supernovae described in Kuznetsova and Connolly (2006). In this method, we consider a limited set of possible supernova types (Branch-normal Ia Branch et al. (1993), Ibc, IIL, IIP, and IIn), and make use of the best currently available supernova models for each type. When improved supernova models are available, they can be easily worked into the method. Using the same notations as in Kuznetsova and Connolly (2006) for the remainder of the paper, we calculate the probability density that the candidate with data $\{A_i\}$ is

[16]This research has made use of the NASA/IPAC Extragalactic Database (NED) which is operated by the Jet Propulsion Laboratory, California Institute of Technology, under contract with the National Aeronautics and Space Administration. Please see http://nedwww.ipac.caltech.edu/ for more information.

Candidate	RA (2000.)	Dec (2000.)	z	δz	source
1	12:37:6.72	62:9:15.84	0.53	0.25	private comm.
2	12:37:1.44	62:11:29.04	0.78	0.005	TKRS
3	12:36:56.16	62:11:56.04	0.83	0.10	private comm.
4	12:37:49.20	62:14:6.72	0.41	0.005	spectrum
5	12:36:21.12	62:11:1.32	0.63	0.005	TKRS
6	12:37:8.16	62:14:25.08	0.56	0.005	TKRS
7	12:37:40.56	62:20:8.16	0.74	0.005	TKRS
8	12:36:16.80	62:14:37.68	0.71	0.10	photo-z
9	12:37:28.32	62:20:39.84	1.14	0.005	spectrum
10	12:36:37.92	62:9:52.92	0.51	0.005	spectrum
11	12:37:24.96	62:13:18.12	0.67	0.005	spectrum
12	12:36:24.48	62:8:35.16	0.95	0.005	spectrum
13	12:36:27.60	62:11:24.36	0.66	0.10	photo-z
14	12:37:19.68	62:18:37.80	1.27	0.005	spectrum
15	12:37:15.12	62:13:33.96	0.90	0.005	spectrum
16	12:36:55.20	62:13:12.36	0.97	0.005	spectrum
17	12:36:33.12	62:13:48.72	0.54	0.10	photo-z
18	12:36:57.84	62:17:24.00	0.97	0.005	TKRS
19	12:36:39.84	62:7:52.68	0.48	0.10	photo-z
20	12:36:31.68	62:8:48.84	0.46	0.10	photo-z
21	12:37:28.80	62:11:28.68	0.94	0.005	spectrum
22	12:37:9.12	62:11:29.40	1.34	0.005	spectrum
23	12:37:12.00	62:12:39.24	0.89	0.10	photo-z
24	12:36:15.93	62:12:37.72	0.29	0.005	spectrum
25	12:37:48.37	62:13:35.50	0.95	0.005	spectrum
26	12:36:26.64	62:6:15.48	1.60	0.12	private comm.
27	12:36:25.92	62:6:55.44	0.64	0.005	spectrum

Table 4: The 27 candidates selected at the end of stage 2 for sample #1.

Candidate	RA (2000.)	Dec (2000.)	z	δz	source
1	12:36:20.88	62:10:20.28	1.10	0.28	private comm.
2	12:36:29.28	62:11:42.36	1.35	0.40	private comm.
3	12:36:19.92	62:13:48.36	0.54	0.13	private comm.
4	12:36:27.20	62:15:9.89	0.74	0.23	private comm.
5	12:36:32.16	62:16:59.52	0.44	0.005	TKRS
6	12:38:3.36	62:17:12.84	0.53	0.20	private comm.
7	12:37:9.36	62:22:15.24	1.61	0.34	private comm.
8	12:37:6.72	62:21:17.64	0.41	0.005	TKRS
9	12:36:26.88	62:8:31.92	0.55	0.20	private comm.
10	12:36:54.24	62:8:24.72	1.45	0.32	private comm.
11	12:36:34.32	62:12:13.32	0.47	0.20	private comm.
12	12:37:33.84	62:19:23.88	0.88	0.38	private comm.
13	12:36:35.04	62:15:51.84	0.85	0.24	private comm.
14	12:36:36.00	62:17:34.80	0.60	0.15	private comm.
15	12:36:55.20	62:13:5.16	0.95	0.28	private comm.
16	12:37:48.24	62:13:36.12	0.89	0.25	private comm.
17	12:36:1.64	62:15:55.70	0.09	0.1	TKRS

Table 5: The 17 candidates selected at the end of stage 2 for sample #2.

Candidate	RA (2000.)	Dec (2000.)	z	δz	source
1	3:32:37.68	-27:46:45.48	1.3	0.005	spectrum
2	3:32:18.70	-27:48:32.69	0.39	0.005	spectrum
3	3:32:48.60	-27:54:15.12	0.84	0.005	spectrum
4	3:32:22.87	-27:51:7.20	0.9	0.1	photo-z
5	3:32:18.24	-27:41:55.32	0.88	0.1	photo-z
6	3:32:13.18	-27:42:5.40	0.42	0.005	spectrum
7	3:32:17.45	-27:46:22.44	0.13	0.1	NED
8	3:32:22.75	-27:51:10.80	0.77	0.12	private comm.
9	3:32:35.92	-27:47:57.95	0.66	0.005	spectrum
10	3:32:42.55	-27:50:24.72	0.58	0.005	spectrum
11	3:32:6.84	-27:44:32.28	1.40	0.005	spectrum
12	3:32:32.62	-27:53:16.44	0.99	0.1	photo-z

Table 6: The 12 candidates selected at the end of stage 2 for sample #3.

Candidate	RA (2000.)	Dec (2000.)	z	δz	source
1	3:32:24.91	-27:46:17.40	1.3	0.005	spectrum
2	3:32:30.07	-27:43:46.56	0.67	0.005	spectrum
3	3:32:22.68	-27:41:52.08	0.53	0.005	spectrum
4	3:32:44.45	-27:55:5.88	1.31	0.005	spectrum
5	3:32:22.46	-27:44:26.16	0.74	0.005	spectrum
6	3:32:5.52	-27:44:27.96	0.91	0.1	photo-z
7	3:32:47.02	-27:54:48.75	1.55	0.005	spectrum
8	3:32:34.75	-27:39:56.16	0.21	0.005	spectrum
9	3:31:58.80	-27:44:58.92	0.58	0.005	spectrum
10	3:32:9.45	-27:41:28.11	0.90	0.1	photo-z

Table 7: The 10 candidates selected at the end of stage 2 for sample #4.

a type Ia supernova at redshift z:

$$P(\mathrm{Ia}|\{A_i\}) = \frac{P(\{A_i\}|\mathrm{Ia})\,P(\mathrm{Ia})}{\sum_T P(\{A_i\}|T)\,P(T)}, \tag{2}$$

where $\{A_i\}$ are the photometric supernova data in some broadband filter a, $P(\{A_i\}|\mathrm{Ia})$ is the probability density to obtain data $\{A_i\}$ for supernova type Ia, $P(\mathrm{Ia})$ contains prior information about type Ia supernovae, the denominator is the normalization over all of the known supernova types T, and both the numerator and the denominator marginalize the supernova parameters $\vec{\theta} \equiv (t_{\mathrm{diff}}, s, M, R_v, A_v)$. The parameters are: t_{diff} is the time difference between the dates of maximum light for the model and the data, t_{diff}; s is the stretch parameter (Perlmutter et al 1997), which parametrizes the width of the light curve (if $T = \mathrm{Ia}$); M is the assumed absolute magnitude in the restframe B-band; and A_v and R_v are the Cardelli-Clayton-Mathis interstellar extinction parameters (Cardelli et al 1998). Note that the denominator also has a marginalization over the entire redshift range considered, $0.0 < \mathrm{z} < 1.7$. We consider T = Branch-normal Ia, Ibc, IIL, IIP, and IIn.

The numerator of Eqn. 2 is thus given by:

$$\sum_{\vec{\theta}} P(\{A_i\}|\vec{\theta},\mathrm{Ia})P(\vec{\theta},\mathrm{Ia}) =$$

$$\frac{\Delta z}{\sqrt{2\pi}\delta z}\, e^{-\frac{(z-\bar{z})^2}{2\delta z^2}}\, \frac{1}{N_T} \sum_{t_{\mathrm{diff}}} \frac{1}{N_{t_{\mathrm{diff}}}} \sum_{R_v,A_v} \frac{1}{N_v} \sum_{M=M_{min}}^{M_{max}} \frac{\Delta M}{\sqrt{2\pi}\delta M}\, e^{-\frac{(M-\bar{M})^2}{2\delta M^2}} \sum_{s=s_{min}}^{s_{max}} \frac{\Delta s}{\sqrt{2\pi}\delta s}\, e^{-\frac{(s-\bar{s})^2}{2\delta s^2}}$$

$$\prod_{i=1}^{n_{epochs}} \frac{\Delta a_j}{\sqrt{2\pi}\delta A_i}\, e^{-\frac{(a_j-A_i)^2}{2\delta A_i^2}}. \tag{3}$$

Note that in contrast to the case considered in Kuznetsova and Connolly (2006), where the redshifts of the candidates were assumed to be perfectly known, we are now introducing an extra term –

a Gaussian prior for the redshift distribution, with a mean $\bar{z}$, a standard deviation of δz, and an increment of $\Delta\ z$. For a supernova of type T that is not a Ia:

$$\sum_{\vec{\theta}} P(\{A_i\}|\vec{\theta},T)P(\vec{\theta},T) = \frac{\Delta z}{\sqrt{2\pi}\delta z}\, e^{-\frac{(z-\bar{z})^2}{2\delta z^2}} \frac{1}{N_T}\sum_{t_{\rm diff}} \frac{1}{N_{t_{\rm diff}}} \sum_{R_v,A_v} \frac{1}{N_v} \sum_{M=M_{min}}^{M_{max}} \frac{\Delta M}{\sqrt{2\pi}\delta M}\, e^{-\frac{(M-\bar{M})^2}{2\delta M^2}} \sum_{s=s_{min}}^{s_{max}} \frac{\Delta s}{s_{max}-s_{min}} \prod_{i=1}^{n_{epochs}} \frac{\Delta a_j}{\sqrt{2\pi}\delta A_i}\, e^{-\frac{(a_j-A_i)^2}{2\delta A_i^2}}. \quad (4)$$

The probability that $\alpha^{\rm th}$ candidate is a type Ia supernova belonging to the $j^{\rm th}$ redshift bin, [$z_{j\,lower}$ - $z_{j\,upper}$], is

$$P_j^\alpha = \int_{z_{j\,lower}}^{z_{j\,upper}} P^\alpha({\rm Ia}|\{A_i\}), \quad (5)$$

and the total number of candidates d_j in the $j^{\rm th}$ bin, as well as the error on this number, are calculated as follows.

Let us suppose that there are a total of N_j candidates in the $j^{\rm th}$ bin, each with its own associated probability P_j^α. Let us define a variable s_α such that $s_\alpha = 1$ if the $\alpha^{\rm th}$ candidate is indeed a type Ia and $s_\alpha = 0$ if it is not, so that there are $k_j \equiv \sum_{\alpha=1}^{N_j} s_\alpha$ type Ia's in this bin. We would like to obtain the best estimate, d_j, of the number of candidates in our sample. Using the Bayes theorem, the probability to measure k_j type Ia's when d_j were expected is given by:

$$P(d_j|k_j) = \frac{P(d_j|k_j)P(k_j)}{\sum_{k_j=0}^{N_j}\sum_{d_j=0}^{\infty} P(d_j|k_j)P(k_j)}, \quad (6)$$

The first term in the numerator of Eqn. 6 is a simple Poisson distribution:

$$P(d_j|k_j) = \frac{d_j^{k_j} e^{-d_j}}{k_j!}, \quad (7)$$

and the second term is

$$P(k_j) \sim \sum_{\{s_\alpha^{k_j}\}} \prod_{\alpha=1}^{N_j} [P_j^\alpha s_\alpha + (1-P_j^\alpha)(1-s_\alpha)], \quad (8)$$

where the sum is over all possible combinations of s_α's that yields a given k_j.

Because we have no way of knowing what k_j is, we must sum over all possible k_j's, or, equivalently, over all possible $\{s_\alpha\}$'s. To obtain the best estimate for d_j, we must maximize the likelihood:

$$L(d_j) = \sum_{\{s_\alpha\}} \frac{d^{k_j} e^{-d_j}}{k_j!} \prod_{\alpha=1}^{N_j} [P_j^\alpha s_\alpha + (1-P_j^\alpha)(1-s_\alpha)] \quad (9)$$

and to evaluate the uncertainty on d_j, we first calculate the full $P(d_j)$

$$P(d_j) = \frac{\sum_{\{s_\alpha\}} \frac{d_j^{k_j} e^{-d_j}}{k_j!} \prod_{\alpha=1}^{N_j} [P_j^\alpha s_\alpha + (1 - P_j^\alpha)(1 - s_\alpha)]}{\sum_{d_j=0}^{\infty} \sum_{\{s_\alpha\}} \frac{d_j^{k_j} e^{-d_j}}{k_j!} \prod_{\alpha=1}^{N_j} [P_j^\alpha s_\alpha + (1 - P_j^\alpha)(1 - s_\alpha)]} \tag{10}$$

and then find the 68% confidence regions for d_j, $[d_j - \sigma_{j\,low}, d + \sigma_{j\,high}]$, by solving:

$$16\% = \sum_{0}^{d_j - \sigma_{j\,low}} P(d_j) = \sum_{d + \sigma_{j\,high}}^{\infty} P(d_j) \tag{11}$$

For a large number of events (*e.g.*, in Monte Carlo samples), it becomes prohibitively expensive to evaluate d_j as given above. We therefore use a simple approximation:

$$d_j = \sum_{\alpha=1}^{N_j} P_j^\alpha, \tag{12}$$

where the uncertainty on d_j is given by:

$$\Delta d_j = \frac{\sum_{\alpha=1}^{N_j} P_j^\alpha}{\sqrt{N_j}} \tag{13}$$

The simplest argument for this assumption is that if all of the probabilities P_j^α were 1 (*i.e.*, the candidates were all known to be type Ia supernovae), using Eqn. 12 would amount to a simple counting of the number of candidates, and Eqn. 13 would become the usual $\sqrt{N}$ error.

We assume that all candidates whose redshift is within $\pm 3\ \delta z$ of the j^{th} bin's boundaries will contribute to this bin. Note that in this formulation, a single candidate with a poorly known redshift may have a probability distribution that spans several redshift bins.

We calculate $P(\mathrm{Ia}|\{A_i\})$ for all 66 candidates. If a given candidates' $P(\{A_i\}|T)\,P(T)$ is less than 10^{-5} for all types T , it is considered to be an "anomaly" and is excluded from further consideration. The 10^{-5} cut was chosen because it is much smaller than the values calculated for simulated supernovae in the Monte Carlo. This method thus excludes any need for the often subjective and time-consuming decision on whether or not a given candidate might be a supernova; all dubious candidates are left in the sample for the probability to decide.

It is a good sanity check to check the contribution of the gold and silver Ia candidates from Riess et al (2004). If the method is working well, they should be among the largest contributors to a given bin. As we showed in Kuznetsova and Connolly (2006), all but one gold Ia candidate (2003eb) do indeed have probabilities ≥ 0.8; 2003eb has only two epochs (epochs 4 and 5 of the GOODS dataset) with "appreciable" SNR (> 10) in both F775W and F850LP bands. All of the gold and silver core-collapse (CC) supernovae from Riess et al (2004) have the probabilities of being Ia's that are close to zero.

3.3.1. Effect of Varying Priors

The statistical errors on the observed number of supernovae N_i are calculated as described in Section 3.3. However, it is important to investigate the effect of varying the assumptions we made for the priors in Eqns. 3 and 4. This procedure yields additional estimates on the errors for N_i. We have performed the following checks:

- **Modified Stretch Prior**. We assumed a Gaussian prior on the stretch parameter for type Ia supernovae:

$$P(s|\mathrm{Ia}) = \frac{e^{-\frac{(s-\bar{s})^2}{2\delta s^2}}}{\sqrt{2\pi}\delta s}\Delta s. \tag{14}$$

  To investigate the effect of this assumption on N_i's, we re-calculate them using a δ-function type stretch prior. In other words, we assume that all type Ia's have a stretch of one.

- **Flat Restframe Absolute Magnitude Prior**. We also assumed a Gaussian prior on the B-band restframe magnitudes for all supernovae:

$$P(M|T) = \frac{e^{-\frac{(M-\bar{M})^2}{2\delta M^2}}}{\sqrt{2\pi}\delta M}\Delta M. \tag{15}$$

  We investigate the effect of this assumption by using a flat magnitude prior; that is, assuming that all magnitudes within $\pm$ 3 δM's are equally likely.

- **No Extinction**. We used three different models for the extinction: one assuming no extinction, one using Cadrelli-Clayton-Mathis parameters A_v, R_v = (0.4, 2.1), and one using A_v, R_v = (0.4, 3.1). While there is no generally accepted model for either A_v or R_v, it is known that A_v peaks sharply at zero (*e.g.*, Hatano et al (1998)). We thus investigate the effect of using the case of no extinction alone and conclude that the answers are not sensitive to the choice of this prior.

- **Modified Prior on the Supernova Rates**. So far, we have assumed a flat prior on the supernova rates. A major obstacle to checking the effect of this assumption is the fact that the rates are not well known, especially at high redshift. Recent work (Dahlen et al. 2004, for example) seems to indicate that the rates of CC supernovae with respect to type Ia's are higher by approximately a factor of 3 at redshifts up to $z \sim$1. We will assume that this ratio holds at all redshifts, and modify the prior accordingly. This does not bias our answer in any way, as we are not making any assumptions about the *absolute* rates of supernovae, but only about their relative rates.

These modifications of the priors generally result in estimates for the number of type Ia's that are lower than those obtained with the "nominal" priors. This is to be expected, since using the more unphysical priors (such as a flat magnitude prior) should result in fewer identified Ia's. We also

find that all of the changes considered contribute roughly equally to the change in the estimated number of Ia's. In other words, there is no single prior that is particularly important; reasonable assumptions should be made for all of them.

We quadratically combine the changes in d_j's due to using different priors. This is a measure of how sensitive d_j's are to the choice of priors. As such, it can be taken as an estimate of the systematic uncertainties.

4. The Rates Calculation

We would like to compute the volumetric type Ia supernova rate in the supernova rest frame, $\mathrm{r_{V,Ia}(z)}$, as a function of redshift z. The expected number of candidates in the j^{th} redshift bin whose center is $\bar{z}_j$ is given by:

$$d_j^{\exp}(z_j) = \frac{r_{V,\mathrm{Ia}}(z_j)}{1+z_j}\,\frac{\Theta}{4\,\pi}\,\frac{dV}{dz}(\bar{z}_j)\left[T_{\mathrm{Ia}}(\bar{z}_j)\epsilon_{\mathrm{Ia}}(z_j) + \frac{r_{V,non-\mathrm{Ia}}(z_j)}{r_{V,\mathrm{Ia}}(z_j)}T_{non-\mathrm{Ia}}(\bar{z}_j)\epsilon_{non-\mathrm{Ia}}(z_j)\right], \qquad (16)$$

where Θ is the survey area covered; dV/dz is the comoving volume computed assuming a ΛCDM cosmology; $T_{\mathrm{Ia}}(z)$ and $T_{non-Ia}(z)$ are the control times for Ia and non-Ia candidates, respectively; ϵ_{Ia} and ϵ_{non-Ia} are the efficiencies of the stage 3 selection for Ia and non-Ia candidates, respectively; and $r_{V,non-Ia}(z)/r_{V,\mathrm{Ia}}(z)$ is the ratio of the non-Ia supernova rate to the Ia supernova rate. Once again, the appearance of this ratio does not bias our results, since we do not make any assumptions about the *absolute* type Ia rate.

The control time T is defined as the the time during which a supernova search is *potentially* capable of finding supernova candidates. In order to calculate it, we simulate HST observations of Branch-normal type Ia and non-type Ia supernovae at redshifts up to 1.7, with the same sampling and exposure times as those of the real data. By shifting the observing grid along the light curves, we calculate the weighted sum of the number of days during which a given supernova could be detected. The weight factors are obtained from the stage 1 efficiency parametrization; it is also required that the light curves satisfy the stage 2 SNR requirements. Therefore, stage 1 and 2 supernova selection efficiencies are naturally built into the control time calculation. However, the stage 3 selection efficiency is *not* part of the control time calculation, and must therefore be computed separately. Calculating the area of the survey is straightforward using a Monte Carlo approach. The calculation of the control time and the survey area is given in Section 4.1.

The selection efficiency ϵ_{Ia} and $\epsilon_{non-\mathrm{Ia}}$ must be calculated for the candidates that passed the control time requirements, and thus satisfy both stage 1 and 2 cuts. We thus create a Monte Carlo sample mimicking real supernova candidates by the time they are ready for the stage 3 typing. We simulate both Ia and non-Ia candidates and calculate the number of candidates as we would for real data. This procedure is described in detail in Section 4.2.

The errors on the expected $d_j^{\exp}$ are a combination of statistical and systematic uncertainties,

with the latter dominating. The systematic uncertainties come from two sources: estimating the variation in $T_{\rm Ia}(z)$ for stretches other than 1, and estimating the effect of varying the ratio of the rates $r_{V,non-Ia}(z)/r_{V,{\rm Ia}}(z)$ between 1 and 3.

4.1. The Control Time and Search Area Calculation

Let us start with describing the calculation of the control time and search area, T and Θ from Eqn. 16. The control time is the time during which a supernova search is in principle capable of finding supernova candidates on the area covered. For the GOODS fields, the orientation of the tiles is such that a candidate is not necessarily accessible for every search epoch due to edge effects (see Fig. 1). For example, for sample 1 from Table 2, a given location may only be covered by epochs 1, 3, and 5 (but not by epochs 2 and 4) of the North GOODS dataset. In both our control time calculation and in the search area calculation, we thus consider all of the possible epoch permutations at each location: 31 possible permutations for samples 1, 3, and 4 and 15 possible permutations for sample 2.

We perform separate control time and search area calculations for the four samples listed in Table 2; however, the approach is the same. For the control time calculation, we make use of the simulation described in some detail in Appendix A of Kuznetsova and Connolly (2006). We use it to create simulated HST observations in both F775W and F850LP bands for Branch-normal type Ia supernovae of stretch 1, as well as for non-type Ia supernovae, at redshifts up to 1.7 with an increment of 0.1. Separate sets of observations are generated for each possible permutations of the available search epochs, for each of the four samples. For example, for a supernova from Sample 1 that happens to be present in every one of the North GOODS epochs, there will be five simulated search observations and a single reference observation. We use typical epoch separations and exposure times for a given sample. The observations are realized using an aperture exposure time calculator with a 0.1" radius. We initially set the explosion date of the supernova on the last date of the available search epoch observation set (*e.g.*, for the supernova example mentioned above it would be on the date the last of the North GOODS data were taken). The observing grid for the search observations is then shifted by one day, and the procedure is repeated $N_{shifts} = 350$ times. For each such shift, we require that the simulated data satisfy both the stage 1 and stage 2 requirements listed in Table 3. The resulting control time thus has the efficiency automatically included. It is given by:

$$T = \sum_{k=1}^{N_{shifts}} \left[1 - \prod_{i=1}^{M} (1 - \epsilon_i^k(SNR_i)) \right] e_k, \tag{17}$$

where the sum is over all the shifts, M is the number of available search epochs (in the example considered above, $M = 5$); ϵ_i^k is a function of the $i^{\rm th}$ subtraction's SNR, parametrized as in Eqn. 1;

and e_k is a binary quantity

$$e_k = \begin{cases} 1 & \text{, if } k^{\text{th}} \text{ shift configuration satisfies stage 2 requirements} \\ 0 & \text{, if } k^{\text{th}} \text{ shift configuration does not satisfy stage 2 requirements} \end{cases} \quad (18)$$

that accesses whether a given configuration has enough epochs with sufficient SNR for the stage 2 selection.

We repeat the control time calculation for Ia's with the stretches of 0.65 and 1.30, and take the larger error between the control time computed for these stretch parameters and that computed for a stretch of 1 as a measure of the systematic error on the control time for Ia's. For reference, Table 8 lists the control time as a function of redshift for both the nominal stretch of 1 and for the stretch of 0.65 and 1.30, for the configurations in which a supernova candidate is assumed present on all of the search epochs.

z	Control time (yrs)											
	Sample #1			Sample #2			Sample #3			Sample #4		
	s=1	s=0.65	s=1.3	s=1	s=0.65	s=1.3	s=1	s=0.65	s=1.3	s=1	s=0.65	s=1.3
0.1	0.84	0.78	0.84	0.84	0.66	0.85	0.68	0.65	0.68	0.30	0.27	0.35
0.2	0.84	0.77	0.84	0.84	0.65	0.85	0.68	0.63	0.67	0.32	0.29	0.42
0.3	0.85	0.77	0.85	0.83	0.64	0.85	0.68	0.63	0.67	0.31	0.28	0.37
0.4	0.84	0.75	0.83	0.80	0.61	0.84	0.67	0.60	0.66	0.32	0.28	0.36
0.5	0.84	0.73	0.84	0.77	0.59	0.84	0.67	0.58	0.66	0.32	0.28	0.36
0.6	0.83	0.72	0.84	0.73	0.56	0.82	0.66	0.57	0.65	0.33	0.28	0.37
0.7	0.81	0.68	0.84	0.69	0.53	0.79	0.63	0.53	0.64	0.32	0.29	0.37
0.8	0.78	0.64	0.83	0.64	0.51	0.75	0.59	0.49	0.63	0.33	0.29	0.37
0.9	0.72	0.59	0.80	0.57	0.46	0.66	0.53	0.43	0.58	0.33	0.28	0.37
1.0	0.68	0.57	0.75	0.54	0.43	0.62	0.48	0.36	0.54	0.33	0.28	0.36
1.1	0.65	0.55	0.72	0.51	0.40	0.59	0.46	0.32	0.49	0.32	0.27	0.37
1.2	0.63	0.53	0.69	0.48	0.35	0.56	0.42	0.27	0.47	0.32	0.26	0.36
1.3	0.60	0.49	0.67	0.46	0.30	0.55	0.38	0.22	0.45	0.32	0.25	0.36
1.4	0.57	0.42	0.64	0.44	0.23	0.53	0.37	0.17	0.43	0.31	0.20	0.36
1.5	0.56	0.36	0.62	0.39	0.15	0.48	0.32	0.13	0.40	0.31	0.17	0.35
1.6	0.51	0.24	0.59	0.34	0.09	0.44	0.27	0.09	0.37	0.26	0.11	0.34
1.7	0.47	0.17	0.56	0.21	0.04	0.38	0.25	0.06	0.33	0.25	0.07	0.31

Table 8: The type Ia control time in years as a function of redshift, for the configurations on which a supernova candidate is assumed to be present on all of the search epochs. The control time is given for three different values of the stretch parameter s: 1 (nominal), 0.65, and 1.30. Note that this control time has the stage 1 and 2 efficiencies built into the calculation.

Note that the control time in Eqn. 16 enters with a factor of $(1 + z)$. This is a consequence of the fact that it is calculated in the observer frame.

Calculating the search area is non-trivial because of the complicated orientations of the GOODS tiles, as well as the overlaps between the tiles (see Fig. 1). In addition, the search area must be calculated separately for all of the possible epoch configurations, as described above. We perform this calculation using a Monte Carlo method. First, we create a grid between the minimum and maximum right ascensions (α) and declinations (δ) covering the entire North or South GOODS area. Then, for a given epoch, and for each point i on the grid, we check whether this (α_i, δ_i) belongs to any of the images that were used to make subtracted data for this epoch. In other words, we convert (α_i, δ_i) into image coordinates (x_j, y_j), and check that: (a) the point falls within the confines of at least one search/reference image pairs; (b) it does not fall on a known bad pixel or a pixel that has been masked off for any other reason (*e.g.*, due to a residual cosmic ray contamination) on either image; and (c) it does not fall into the gap between the two ACS chips on the search image. If all of these requirements are satisfied, the point is counted toward the area calculation. Once counted, a given point can never again be counted in for this particular epoch. This avoids double-counting, an issue particularly important since most GOODS tiles overlap at least somewhat with their immediate neighbors, and a point with a given (α_i, δ_i) may well be present on several images. A separate accounting is kept for the number of points for all the different epoch permutations. For example, let us suppose that the number of points that cover all five of the GOODS North epochs is $d1$, and that the number of total points tried in the grid is D_1; then the area corresponding to this configuration is $A\,d_1/D_1$, where A is the area of the entire North GOODS survey.

Figure 3 shows the resulting control time times surveyed area ($\Theta\,T(z) = \sum_{i=1}^{n} \Theta_i(z)\,T_i(z)$, where n is the number of all possible permutations) for stretch 1 type Ia's, as a function of redshift for the four different samples in Table 2. There are several interesting features in Fig. 3. First, the control time times area decreases with redshift for all four samples. This is a consequence of the fact that it becomes more difficult to satisfy the stage 2 SNR requirements for higher redshift (dimmer) supernovae. Second, for a given redshift, the control time times area is smaller for sample #2 than for sample #1, a consequence of the fact that there are only 4 search epochs in sample #2 vs. 5 search epochs in sample #1. Third, the control time times area is distinctly smaller for the South GOODS samples (samples #3 and #4) than for either of the North samples (#1 and #2), a reflection of the fact that for these samples we are forced to use references made from two of the GOODS South dataset's own epochs. Finally, the control time times area is smaller for sample #4, which uses epochs 1+2 of the GOODS South dataset as its reference data, than for it is for sample #5, which uses epochs 4+5. This is simply because the rise time of a supernova is smaller than its decline time.

4.2. Calculating $\epsilon_{\rm Ia}$ and $\epsilon_{non-{\rm Ia}}$

In order to find out the efficiency of the stage 3 selection, we generate four Monte Carlo datasets mimicking the data from the four datasets listed in Table 2 (in other words, they have the same

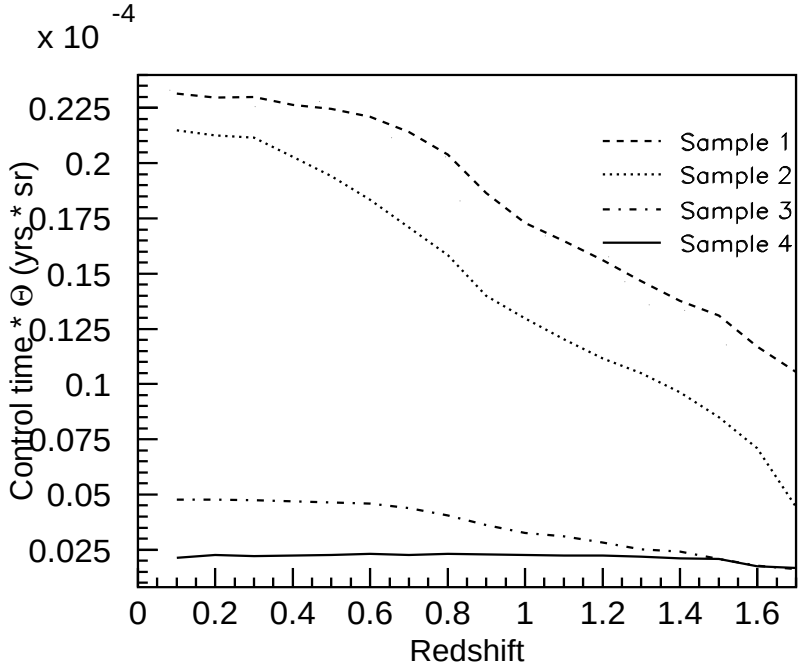

Fig. 3.— The control time times surveyed area as a function of redshift for the four samples listed in Table 2, calculated for a stretch 1 Branch-normal Ia. The dashed line is for sample #1, where the 5 GOODS North epochs were used as the search data, and the combined Search2004 sample, as the reference. The dotted line is for sample #2, where the 4 epochs of the Search2004 dataset were used as the search data, and the combined GOODS North data, as the reference. The dashed-dotted line is for sample #3, where all 5 epochs of the GOODS South sample were used as the search data; and the combined epochs 4+5 of the South GOODS dataset, as the reference. The solid line is for sample #4, where all 5 epochs of the GOODS South sample were used as the search data; and the combined epochs 1+2 of the South GOODS dataset, as the reference.

sampling, exposure times, *etc.*, as the data). Each Monte Carlo dataset contains 500 candidates for each of the 5 supernova types considered (Branch-normal Ia, Ibc, IIL, IIP, and IIn). The redshifts of these candidates are drawn from a Gaussian distribution that uses the redshifts and redshift errors of the real data events; the exposure times and sampling intervals also mimic those of the real data. The candidates' rest-frame B-band magnitudes, stretch (for type Ia's), and extinction parameters are drawn from the appropriate distributions used in Eqns. 3 and 4. The time period between the date of explosion and the first observation is randomly drawn from a flat distribution. In addition, because we are simulating a dataset as it would appear by the time it is ready for the stage 3 selection, we impose the same selection requirements from stages 1 and 2 on these Monte

Carlo events as we do on the real data.

After these Monte Carlo samples are generated, we calculate the number of candidates in each redshift bin. Dividing this number by the total number of the generated Ia's yields the efficiency $\epsilon^m_{j\,\mathrm{Ia}}$, for redshift bin m for Monte Carlo dataset m. Similarly, the efficiency for non-type Ia candidates, $\epsilon^m_{j\,non-\mathrm{Ia}}$, is defined as the sum of the probabilities of the non-type Ia candidates divided by the total number of all generated non-type Ia supernovae.

4.3. Comparison of Expected and Observed Numbers of Supernovae

We can now put everything together and compute the expected numbers of supernovae for a given model of the type Ia supernova rates using Eqn. 16. One must be careful at this stage about the choice of redshift binning. For the purposes of comparing our results with previously published work, especially that of Dahlen et al. (2004), we can choose four redshift bins $0.2 \leq z < 0.6$, $0.6 \leq z < 1.0$, $1.0 \leq z < 1.4$, and $1.4 \leq z < 1.7$. This comparison is carried out in Section 4.4; However, using any binning assumes the knowledge of the behavior of the rates over the width of the bin. The four bins listed above may be too wide to be confident of this assumption. Nevertheless, the uncertainty in the candidates' redshifts forces us to use finite bins; we choose the width of the bins to be $\Delta z = 0.1$. Table 9 lists the numbers of observed candidates in these bins.

Redshift bin	d^1_j	d^2_j	d^3_j	d^4_j
$0 \leq z < 0.1$	$0.00^{0.00}_{0.00} \pm 0.00$	$0.00^{0.00}_{0.00} \pm 0.00$	$0.00^{0.00}_{0.00} \pm 0.00$	$0.00^{0.00}_{0.00} \pm 0.00$
$0.1 \leq z < 0.2$	$0.00^{0.00}_{0.00} \pm 0.00$	$0.00^{0.00}_{0.00} \pm 0.00$	$0.00^{0.00}_{0.00} \pm 0.00$	$0.00^{0.00}_{0.00} \pm 0.00$
$0.2 \leq z < 0.3$	$0.16^{0.07}_{0.07} \pm 0.16$	$0.00^{0.00}_{0.00} \pm 0.01$	$0.00^{0.00}_{0.00} \pm 0.00$	$0.00^{0.00}_{0.00} \pm 0.00$
$0.3 \leq z < 0.4$	$0.37^{0.13}_{0.13} \pm 0.26$	$0.29^{0.08}_{0.08} \pm 0.13$	$0.00^{0.00}_{0.00} \pm 0.00$	$0.00^{0.00}_{0.00} \pm 0.00$
$0.4 \leq z < 0.5$	$1.49^{0.47}_{0.47} \pm 1.00$	$1.27^{0.33}_{0.33} \pm 0.15$	$0.00^{0.00}_{0.00} \pm 0.00$	$0.00^{0.00}_{0.00} \pm 0.00$
$0.5 \leq z < 0.6$	$3.07^{0.92}_{0.92} \pm 0.89$	$0.25^{0.07}_{0.07} \pm 0.05$	$0.01^{0.01}_{0.01} \pm 0.01$	$1.00^{1.00}_{1.00} \pm 1.00$
$0.6 \leq z < 0.7$	$4.01^{1.27}_{1.27} \pm 2.80$	$0.26^{0.07}_{0.07} \pm 0.16$	$0.03^{0.02}_{0.02} \pm 0.04$	$0.00^{0.00}_{0.00} \pm 0.00$
$0.7 \leq z < 0.8$	$1.52^{0.57}_{0.57} \pm 0.68$	$1.96^{0.52}_{0.52} \pm 0.46$	$0.13^{0.08}_{0.08} \pm 0.16$	$0.00^{0.00}_{0.00} \pm 1.00$
$0.8 \leq z < 0.9$	$2.51^{0.84}_{0.84} \pm 0.39$	$1.76^{0.47}_{0.47} \pm 0.37$	$0.30^{0.15}_{0.15} \pm 0.55$	$0.00^{0.00}_{0.00} \pm 0.02$
$0.9 \leq z < 1.0$	$0.14^{0.07}_{0.07} \pm 0.22$	$1.11^{0.30}_{0.30} \pm 0.37$	$1.10^{0.64}_{0.64} \pm 0.75$	$0.12^{0.12}_{0.12} \pm 0.14$
$1.0 \leq z < 1.1$	$1.09^{0.54}_{0.54} \pm 0.18$	$1.11^{0.31}_{0.31} \pm 0.44$	$0.96^{0.55}_{0.55} \pm 0.43$	$0.62^{0.62}_{0.62} \pm 0.60$
$1.1 \leq z < 1.2$	$1.10^{0.64}_{0.64} \pm 0.12$	$0.63^{0.19}_{0.19} \pm 0.23$	$0.01^{0.01}_{0.01} \pm 0.02$	$0.38^{0.38}_{0.38} \pm 0.21$
$1.2 \leq z < 1.3$	$1.12^{0.79}_{0.79} \pm 0.08$	$0.68^{0.23}_{0.23} \pm 0.11$	$1.00^{0.71}_{0.71} \pm 0.00$	$0.96^{0.68}_{0.68} \pm 0.41$
$1.3 \leq z < 1.4$	$0.47^{0.47}_{0.47} \pm 0.11$	$0.43^{0.14}_{0.14} \pm 0.09$	$1.00^{1.00}_{1.00} \pm 0.00$	$0.93^{0.93}_{0.93} \pm 0.39$
$1.4 \leq z < 1.5$	$0.51^{0.51}_{0.51} \pm 0.13$	$0.53^{0.18}_{0.18} \pm 0.21$	$0.00^{0.00}_{0.00} \pm 0.00$	$0.00^{0.00}_{0.00} \pm 0.00$
$1.5 \leq z < 1.6$	$0.20^{0.20}_{0.20} \pm 0.06$	$0.33^{0.12}_{0.12} \pm 0.25$	$0.00^{0.00}_{0.00} \pm 0.00$	$0.00^{0.00}_{0.00} \pm 0.00$
$1.6 \leq z < 1.7$	$0.00^{0.00}_{0.00} \pm 0.00$	$0.12^{0.04}_{0.04} \pm 0.13$	$0.00^{0.00}_{0.00} \pm 0.00$	$0.00^{0.00}_{0.00} \pm 0.00$

Table 9: The number of observed candidates d^m_j in $\Delta z = 0.1$ redshift bins (j = [1,..,17]), for the four samples listed in Table 2 (m = [1,..,4]). The errors are statistical (asymmetric) and systematic, respectively.

We calculate the observed numbers of supernovae for redshifts $z \leq 1.7$, as well as the expected numbers of supernovae for several different models of the rates: z-independent, evolving with z as a power law, and a model related to the SFH. We perform a Levenberg-Marquardt least-squares fit of the observed numbers of supernovae to the predictions for all the three models. For the fitting purposes, we combine the statistical and systematic errors on the data. We use the IDL function MPFIT, which we modified for the case of asymmetric input errors.

- **Redshift-independent rate.** Assuming the rate is flat as a function of redshift, we obtain the best-fitted value of $r_{V,Ia_{\bar{z}=0.88}} = (1.50 \pm 0.09) \times 10^{-4}\ N_{Ia}/(\mathrm{sr\ year\ Mpc^3}\ h_{70}^{-3})]$), for a mean redshift $\bar{z}$, with a $\chi^2 = 15.48$ for 16 degrees of freedom. In other words, a redshift-independent rate is a fairly good fit to our data. Figure 4 shows the resulting distribution of the predicted and observed numbers of supernovae. The errors on both the observed and predicted numbers of supernovae are a conservative quadratic combination of the statistical and systematic errors. For the predicted numbers of supernovae, the systematic errors dominate.

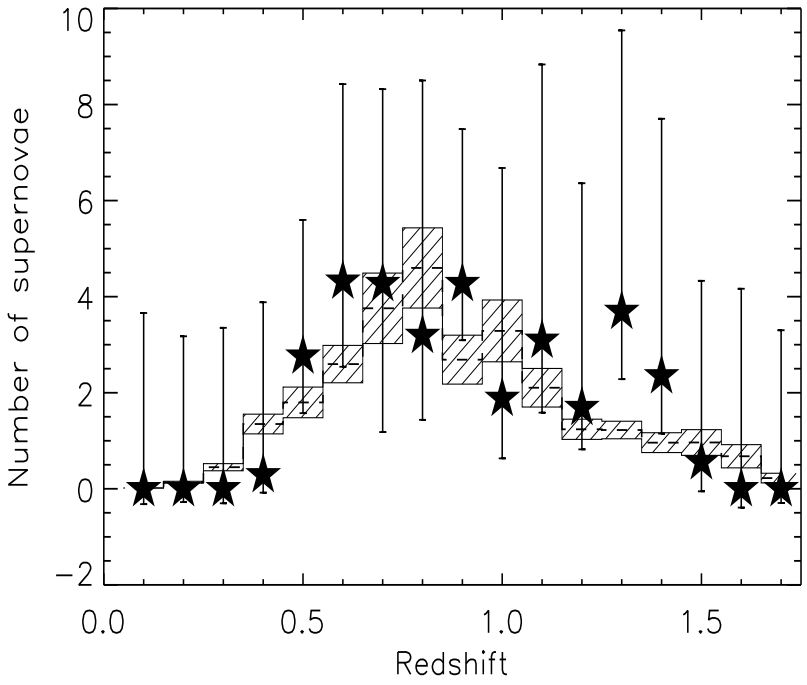

Fig. 4.— The observed (filled stars) and predicted (dashed histogram) numbers of supernovae as a function of redshift assuming a flat rate of $r_{V,Ia_{\bar{z}=0.90}} = 1.50 \times 10^{-4}\ N_{Ia}/(\mathrm{sr\ year\ Mpc^3}\ h_{70}^{-3})]$). The shaded region around the predicted numbers indicates the range of combined statistical and systematic errors.

- **Rate evolving as a power law with redshift.** Assuming the rate is varying as a function of redshift as $(1 + z)^{\alpha}$, we obtain the best-fitting value for $\alpha = (1.83^{+}1.08\_1.08)$, with a χ^2 = 10.56 for 15 degrees of freedom. This is consistent with Pain et al. (2002), who found $\alpha = 0.8^{+}1.6\_1.6$.

- **Rate related to the SFH.** A particularly interesting aspect of a type Ia supernova rates analysis is the possibility of constraining the delay time between the formation of a progenitor star and a supernova explosion, which in turn helps constrain possible models for the type Ia supernova formation. Recently, it has been suggested (Mannucci et al 2006) that the delay function may be bimodal, with one component responsible for the "prompt" type Ia supernovae that explode soon after the formation of their progenitors; and the other, for the "tardy" supernovae that have a much longer delay time. Following this model, the type Ia supernova rate can be represented as:

$$\mathrm{r_{V,Ia}(z)} = A\rho_*(z) + B\dot{\rho}_*(z), \tag{19}$$

  where $\dot{\rho}_*(z)$ is the instantaneous star formation history, and $\rho_*(z)$ is the integrated SFH. The first term of the equation accounts for the "tardy" population, while the second, for the "prompt" one. We use the parametric form of the SFH as given in Hopkins and Beacom (2006):

$$\dot{\rho}_*(z) = \frac{(a + bz)\, h_{70}}{1 + (z/c)^d}, \tag{20}$$

  where $h_{70} = 0.7$, $a = 0.017$, $b = 0.13$, $c = 3.3$, $d = 5.3$. The results of our fit give $A = (0.0 \pm 7.4) \times 10^{-14}$ yr^{-1}M$_{\odot}^{-1}$ and $B = (2.4 \pm 0.8) \times 10^{-3}$ yr^{-1}/(M$_{\odot}$ yr^{-1}), with a $\chi^2 = 10.15$ for 15 degrees of freedom. We will return to this model in Section 4.4.

It is apparent from this exercise the available data are in fact incapable of definitively selecting one model out of the ones considered. The quality of the fits, as given by the χ^2 per degree of freedom, is equally good for all three models.

4.4. Comparison of the Calculated Rates with the Literature

For comparing our results with those of Dahlen et al. (2004), we now compute the type Ia supernova rates in four redshift bins, $0.2 \leq z < 0.6$, $0.6 \leq z < 1.0$, $1.0 \leq z < 1.4$, and $1.4 \leq z < 1.7$. Table 10 enumerates the estimates for the number of candidates in these redshift bins for the four samples listed in Table 2.

Using all four samples, we compute the weighted averages of the rates for each bin, using a quadratic combination of the statistical and systematic errors as the weights. The values for $\Theta T(z)$, dV/dz, and z in Eqn. 16 are taken in the middle of the bin. The resulting rates are summarized in Table 11.

Redshift bin	d_j^1	d_j^2	d_j^3	d_j^4	Total
$0.2 \leq z < 0.6$	$1.88^{0.57}_{0.57} \pm 1.26$ (0)	$1.62^{0.41}_{0.41} \pm 0.21$ (0)	$0.01^{0.00}_{0.00} \pm 0.01$ (0)	$1.00^{1.00}_{1.00} \pm 1.00$(2)	4.50
$0.6 \leq z < 1.0$	$10.36^{2.51}_{2.51} \pm 3.54$ (6)	$3.79^{1.01}_{1.01} \pm 1.01$ (0)	$0.51^{0.36}_{0.36} \pm 1.51$ (2)	$0.12^{0.12}_{0.12} \pm 1.10$ (2)	14.15
$1.0 \leq z < 1.4$	$3.38^{1.20}_{1.20} \pm 0.40$ (3)	$2.24^{0.62}_{0.62} \pm 0.44$ (0)	$1.96^{0.98}_{0.98} \pm 0.43$ (1)	$1.71^{1.21}_{1.21} \pm 0.86$ (1)	9.02
$1.4 \leq z < 1.7$	$0.86^{0.86}_{0.86} \pm 0.11$ (0)	$0.78^{0.26}_{0.26} \pm 0.46$ (0)	$0.00^{0.00}_{0.00} \pm 0.00$ (1)	$0.00^{0.00}_{0.00} \pm 0.00$ (1)	1.62

Table 10: The number of observed candidates d_j^m in four redshift bins (j = [1,..,4]), for the four samples listed in Table 2 (m = [1,..,4]). The errors are statistical and systematic, respectively. The numbers in parenthesis are the number of gold and silver Ia's in the sample from Riess et al (2004).

Redshift bin	$r_{V,Ia}(z)$ ($[10^{-4}\ N_{Ia}/(\text{sr year Mpc}^3\ h_{70}^{-3})]$)
$0.2 \leq z < 0.6$	0.60 ± 0.16
$0.6 \leq z < 1.0$	0.88 ± 0.25
$1.0 \leq z < 1.4$	0.67 ± 0.26
$1.4 \leq z < 1.7$	0.92 ± 0.71

Table 11: The type Ia supernova rates in the four redshift bins considered. The errors are a quadratic combination of the statistical and systematic errors.

The methods used in our work for identifying and classifying supernovae, for computing the efficiency, the control time, and the area of the survey are completely different from those used in Dahlen et al. (2004). A major potential source of the difference in results is the fact that for all of the components of the analysis that rely on the use of supernova templates we use the templates that include both the UV (rest frame wavelength < 3460 Å) and IR (rest frame wavelength > 6600 Å) regions. Moreover, our calculation of the control time carefully takes into account the observing conditions for the four samples considered and sums over every possible observing configuration.

In Section 4.3, it was clear that our data sample alone has a fairly low number of supernovae at lower redshifts. In order to anchor the fit at low redshifts, we now add the results of Cappellaro et al. (1999), Madgwick et al. (2003), and Blanc et al. (2004) to our results. The Levenberg-Marquardt least-squares fit of the data to the model of Eqn. 19 is shown in Fig. 5. We obtain $A = (1.42 \pm 0.70) \times 10^{-14}$ yr^{-1}M$_\odot^{-1}$ and $B = (0.65 \pm 0.18) \times 10^{-3}$ yr^{-1}/(M$_\odot$ yr^{-1}). These results are entirely consistent with those obtained by Neill et al. (2006): $A = (1.4 \pm 1.0) \times 10^{-14}$ yr^{-1}M$_\odot^{-1}$ and $B = (8.0 \pm 2.6) \times 10^{-4}$ yr^{-1}/(M$_\odot$ yr^{-1}). The χ^2 of the fit is 4.15 for 5 degrees of freedom. Several features are apparent in Fig. 5:

- The contribution from the integrated SFH is consistent with zero.
- The previously published rates are statistically consistent with our best-fitting model with the exception of the results of Barris and Tonry (2006) at $z = 0.55$, 0.65, and 0.75, where

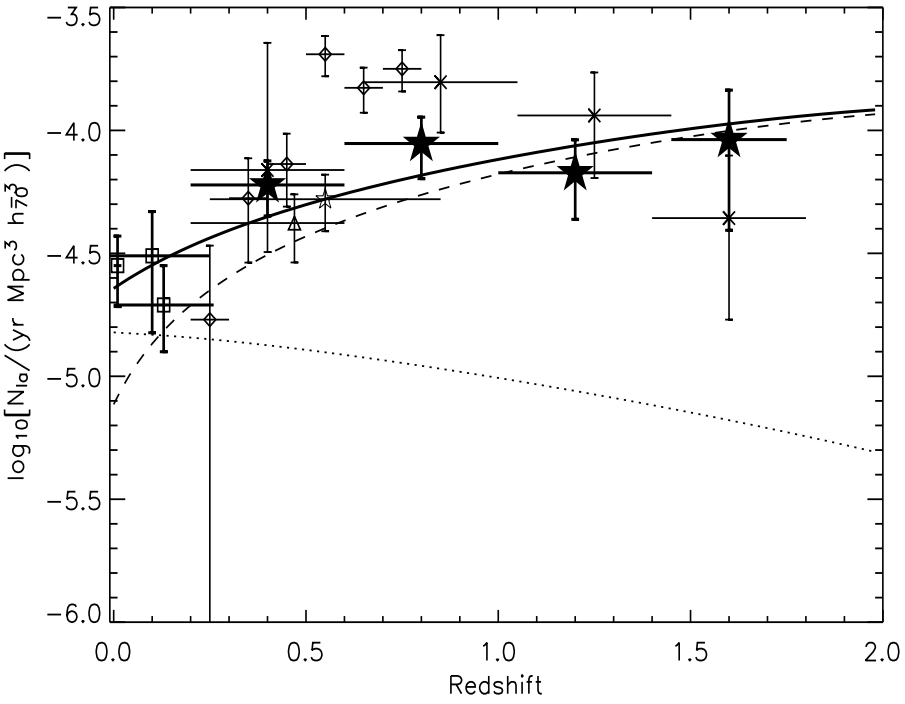

Fig. 5.— The least-square fit of our data (empty triangles) to the two-component model. The dashed line represents the prompt component that is proportional to the instantaneous SFH. The dotted line represents the tardy component that is proportional to the integrated SFH. The thick solid line is the sum of the two. The first three empty squares at low redshifts are, from lower to higher redshifts, the results of Cappellaro et al. (1999), Madgwick et al. (2003), and Blanc et al. (2004), respectively, The empty upturned triangle at $z = 0.47$ is from Neill et al. (2006). The empty star at $z = 0.55$ is from Pain et al. (2002). The empty diamonds are the results of Barris and Tonry (2006). The crosses are from Dahlen et al. (2004). The filled stars are the results of this work. The fit used our results combined with those of Cappellaro et al. (1999), Madgwick et al. (2003), and Blanc et al. (2004). The horizontal bars are estimated redshift bin sizes.

the discrepancy is at the level of 4.0, 2.9, and 5.2 σ, respectively. It has been argued in Neill et al. (2006) (who also noted that the results of Barris and Tonry (2006) beyond the redshift of 0.5 appear to be rather high) that contamination by non-type Ia's is the most likely source of the problem.

It was suggested in Dahlen et al. (2004) and Strolger et al. (2004) that the Ia rate is a convolution of the SFH and a Gaussian time delay distribution function with a characteristic time delay $\tau \sim$3 Gyr and a $\sigma = 0.2\ \tau$. While it is already clear from the discussion in Section 4.3 that

our data are in fact consistent with a wide range of models, we consider the Gaussian delay model as well for the sake of completeness. We fit our results, combined with those of Cappellaro et al. (1999), Madgwick et al. (2003), and Blanc et al. (2004), to such a model, using the Hopkins-Beacom SFH. We obtain that the best-fitting parameters are $\tau = (2.47 \pm 2.47)$ Gyr and $\sigma = (0.46 \pm 1.11)$ τ, with a fit χ^2 of 2.85 for 4 degrees of freedom. The fit is shown in Fig. 6.

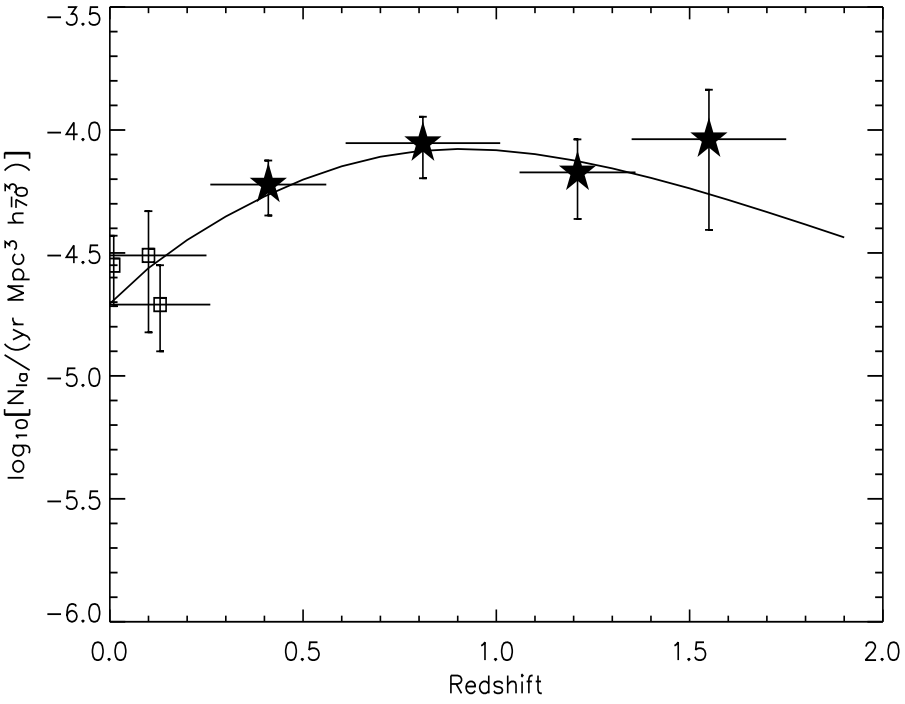

Fig. 6.— The best-fit model of the Gaussian time delay model to our results (filled stars), combined with those of Cappellaro et al. (1999), Madgwick et al. (2003), and Blanc et al. (2004) (empty squares), from lower to higher redshifts, respectively. The horizontal bars are estimated redshift bin sizes.

One of the main implications of this model is the drop-off of the rates at higher redshifts. We find no conclusive evidence for this scenario. More high redshift supernova data are needed to definitively resolve the controversy.

5. Conclusions

We have analyzed the rates of type Ia supernovae up to a redshift of 1.7 using two samples collected with the HST: the GOODS data, and the Search2004 sample collected in the Spring-

Summer 2004 covering the GOODS North field. Using only the data from two broadband filters, F775W and F850LP, we applied a novel technique for identifying type Ia supernovae based on a Bayesian probability approach.

Our analysis has several distinct differences from that of Dahlen et al. (2004), who also analyzed the GOODS dataset. Apart from the usage of the Bayesian approach for identifying type Ia supernovae, we make use of the full supernova templates extending both to the UV and IR parts of the spectrum in the supernova restframe. We use these templates for typing supernovae, as well as for calculating the efficiency of our supernova search, and the control time. The calculations of the supernova finding efficiency, the control time, and the survey area are all done taking into account the specific observing configurations pertinent for the surveys, such as exposure times, cadences, the orientations of the GOODS tiles, *etc.*.

It must be pointed out that we have used the best currently available models to create the lightcurve templates for five different supernova types. These templates will undoubtedly be improved over the next several years as more supernova data becomes available. The existing and upcoming supernova cosmology experiments will not only help better understand the known supernova types, but also most likely yield discoveries of new supernova species, which can then be added to the Bayesian classification framework. Likewise, a better understanding of the many parameters that affect supernova observations (*e.g.*, the interstellar dust), will improve the classification scheme.

For comparison with previous work, we calculated the type Ia supernova rates in four redshift bins, $0.2 \leq z < 0.6$, $0.6 \leq z < 1.0$, $1.0 \leq z < 1.4$, and $1.4 \leq z < 1.7$, and fitted the resulting rates to a two-component model in which type Ia supernovae come from two distinct populations: one that essentially traces the instantaneous SFH, while the other is proportional to the integrated SFH. Parametrizing the latter contribution by parameter A, and the former, by parameter B, we find $A = (1.42 \pm 0.70) \times 10^{-14}$ yr^{-1}M$_{\odot}^{-1}$ and $B = (0.65 \pm 0.18) \times 10^{-3}$ yr^{-1}/(M$_{\odot}$ yr^{-1}). It is therefore apparent that the contribution from the integrated SFH component is consistent with zero. Note, however, that because the calculation of the rates in large redshift bins is problematic, the above results are given mostly for ease of comparison with previously published work and should be taken with a grain of salt.

We also carried out a comparison of the predicted and observed numbers of supernovae in small redshift bins of 0.1, for several different models of the type Ia supernova rates: a redshift-independent rate, a power-law redshift-dependent rate, and a rate related to the SFH (as described above). We find that the data fits all three models equally well. One implication of this conclusion is that we find no conclusive evidence for the suggested drop-off of the supernova rates at high redshifts. However, more high redshift rate measurements are needed to definitively settle the question.

6. Acknowledgments

We would like to thank Tomas Dahlen and Bahram Mobasher for providing us with photometric redshifts for a number of supernova candidates. We are especially grateful to Brian Connolly who made invaluable contributions, particularly to the more statistics-oriented parts of the paper. Without his help this work would never have been finished. We gratefully acknowledge using Hubble Space Telescope data from programs GO-9583, GO-9425, GO-9727, and GO-9728. Financial support for this work was provided by NASA through program GO-9727 from the Space Telescope Science Institute, which is operated by AURA, Inc., under NASA contract NAS 5-26555. This work was also partially supported by the Director, Office of Science, Department of Energy, under grant DE-AC02-05CH11231.

REFERENCES

G. Aldering *et al.*, PASP

E. Baron *et al.*, ApJ 616, 91 (2004)

B. J. Barris and J. L. Tonry, ApJ 637, 427 (2006)

E. Berin and S. Arnouts, A&A 117, 393 (1996)

G. Blanc *et al.*, A&A 423, 881 (2004)

D. Branch, A. Fisher, P. Nugent, AJ 106, 2383 (1993)

J. A. Cardelli, G. C. Clayton, and J. S. Mathis, ApJ 329, L33 (1988)

E. Cappellaro, R. Evans, and M. Turatto, A&A 351, 459 (1999)

S. Chandrasekhar, ApJ 74, 81 (1931)

A. Fruchter and R. N. Hook, PASP 114, 144 (2002).

T. Dahlen *et al.*, ApJ 613, 189 (2004)

M. Dickinson *et al.*, in the proceedings of the ESO/USM Workshop "The mass of Galaxies at Low and High Redshift" (Venice, Italy, October 2001), eds. R. Bender and A. Renzini (2003).

M. Giavalisco *et al.*, ApJ 600, L93 (2004)

D. Hardin *et al.*, A&A 362, 419 (2000)

K. Hatano, D. Branch, and J. Deaton, ApJ 502, 177 (1998)

A. M. Hopkins and J. F. Beacom, accepted for publication in ApJ, preprint astro-ph/0601463 (2006)

S. Perlmutter *et al.* (The SCP Collaboration), ApJ 483, 565 (1997)

A. G. Riess *et al.*, AJ 116, 1009 (1998)

J. Krist and R. Hook, "The TinyTim User's Guide", STScI, 339 (2004)

N. Kuznetsova and B. Connolly, accepted for publication in ApJ, preprint astro-ph/0609637 (2006)

J. D. Neill *et al.* 2006

E. V. Linder and D. Huterer, Phys. Rev. D67, 081303 (2003)

D. S. Madgwick *et al.*, ApJ 599, L33 (2003)

F. Mannucci, M. Della Valle, N. Panagia, MNRAS 370, 773 (2006)

B. Mobasher, T. Dahlen, private communications.

R. Pain *et al.*, ApJ 577, 120 (2002)

A. Renzini *et al.*, in the proceedings of the ESO/USM Workshop "The mass of Galaxies at Low and High Redshift" (Venice, Italy, October 2001), eds. R. Bender and A. Renzini (2003)

A. G. Riess *et al.*, 2004

J. L. Tonry *et al.*,ApJ 594, 1 (2003)

L.-G. Strolger *et al.*, ApJ 613, 200 (2004)

N. Suzuki *et al.*, in preparation (2007)

P. G. Van Dokkum, PASP 113, 1420 (2001)

G. D. Wirth *et al.*, AJ 127, 3121 (2004)